Hierarchical structure of microbial cellulose and marvelous water uptake, investigated by combining neutron scattering instruments at research reactor JRR-3, Tokai

by Ananda Putra

Submission date: 22-May-2023 02:21PM (UTC+0700)
Submission ID: 2099025519
File name: polymer_176_pp244-255_th2019.pdf (3.58M)
Word count: 8758
Character count: 43494

Polymer 176 (2019) 244–255

Contents lists available at ScienceDirect

Polymer

journal homepage: www.elsevier.com/locate/polymer

Hierarchical structure of microbial cellulose and marvelous water uptake, investigated by combining neutron scattering instruments at research reactor JRR-3, Tokai

Satoshi Koizumi[a,*], Yue Zhao[b], Ananda Putra[b]

[a] Research Laboratory of Living Soft Matter, Beam Line Science Course, Institute of Quantum Beam Science, Ibaraki University, Japan
[b] Quantum Beam Science Centre, Japan Atomic Energy Agency, Ibaraki, 319-1195, Japan

HIGHLIGHTS

- In the previous literatures [*Eur. Phys. J. E*, 2008 and *Macromol. Symp.* 2009], we elucidated that 90% of total water is accumulated in non-crystalline bundle in microbial cellulose (MC) produced by *Acetobacter Xylinum*.
- In this paper, we developed our arguments by newly adding the knowledges on (i) the hierarchy in a bacterium body studied by SANS & USANS and (ii) the non-crystalline local structure in as-produced MC in a culture solution, confirmed by neutron diffraction with polarization analyses.
- As a control, we studied a synthetic polymer gel of poly(*N*-isopropylacrylamide) (PNIPAAm) in a swollen state.
- A mechanism of excellent water absorption of MC is attributed to ***capillarity*** related to hierarchically preserved non-crystalline domains, whereas tight hydration onto a monomer unit via a hydrogen bond is crucial for high water absorption for the PNIPAAm gel.

ARTICLE INFO

Keywords:
Small-angle neutron scattering
Ultra-small-angle neutron scattering
Hierarchical structure
Microbial cellulose

ABSTRACT

We discuss microbial cellulose (MC) produced by *Acetobacter Xylinum* and its metabolism related to the bacterium body structure on a basis of knowledges obtained by the small-angle scattering method with combining different spectrometers. MC is a supra-molecule system impregnated with a huge amount of water about 99% by weigh. In the previous literature [*Eur. Phys. J. E*, 2008 and *Macromol. Symp.* 2009], we elucidated that 90% of total water is accumulated in non-crystalline bundle causing concentration fluctuations. In this paper, we develop our arguments by newly adding the knowledges on (i) the hierarchy in a bacterium body studied by SANS & USANS and (ii) the non-crystalline local structure in as-produced MC in a culture solution, confirmed by neutron diffraction with polarization analyses. As a control to emphasize the peculiarity of MC, we compare MC to a synthetic polymer gel of poly(*N*-isopropylacrylamide) (PNIPAAm) in a swollen state. Consequently, we conclude that a mechanism of excellent water absorption found for MC is attributed to ***capillarity*** related to hierarchically preserved non-crystalline domains, whereas tight hydration onto a monomer unit via a hydrogen bond is crucial to result in high water absorption for the PNIPAAm gel.

1. Introduction

Soft matters, in a multi-component system with various sizes, are assembled to form a hierarchical structure, the size of which ranges from atomic size to micron meters. They function sensitively in a response to stimuli, such as changing temperature or humidity, irradiating light, imposing deformation and pressure. Interestingly, we notice that a crossover from materials to life occurs in the length scales between 100 nm and 1 μm (sub microns), which corresponds to the length scales covered by "ultra-small-angle scattering". Fig. 1 [1] shows a photo obtained by transmission electron microscope (TEM) detecting an instant that a gram negative and prokayotic bacterium (*Acetobactor xylinum*) produces microbial cellulose (MC) fibers from its body. The length of bacterium is about several μm. In this paper, we aim to investigate MC, on a basis of knowledges obtained by the combining neutron scattering methods; using small-angle neutron scattering (SANS) & ultra-small-angle neutron scattering (USANS) and triple-axis (TAS) neutron scattering with polarization analysis. In the previous

* Corresponding author.
E-mail address: satoshi.koizumi.prof@vc.ibaraki.ac.jp (S. Koizumi).

https://doi.org/10.1016/j.polymer.2019.05.022
Received 4 October 2018; Received in revised form 5 May 2019; Accepted 8 May 2019
Available online 12 May 2019
0032-3861/

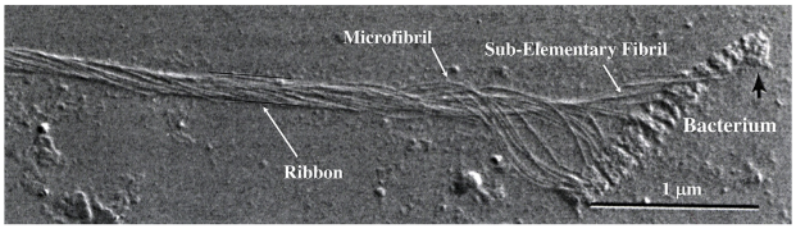

Fig. 1. Transmission electron micrograph showing an instant of bacterium and microbial cellulose fibers from its body. The hierarchical structure of microbial cellulose (sub-elementary fibrils, microfibrils and ribbon) is detected (C. H. Haigler, Copyright, Marcel Dekker, Inc.)..

works by SANS and USANS [2–4], we discussed that the hierarchical structure for the as-produced MC, referred to "*pellicle*", which storages a huge amount of water closer to 99% by weight as the usual synthetic hydrogels. Water exchange or drying process was also investigated by time-resolved SANS measurements [5,6]. In this paper, we discuss the hierarchical structure of MC in the relation with the bacterium body structure and its metabolism.

Cellulose is a linear homo polysaccharide with a high level of symmetry of an amphiphile molecular structure [7,8]. The intra-chain hydrogen bonding makes a cellulose chain stiff and plane so that natural cellulose generally tends to be crystalline and insoluble to water or organic chemicals. The excellent affinity to water, found for MC, is tightly related to its non-crystalline self-assembled structure, which is hierarchically weaved by the bacterium. The formation of hierarchical non-crystalline structure of the pellicle is initiated by a nearly simultaneous and subsequent processes of polymerization, crystallization and molecular assembly, which occur in or in the vicinity of the cell membrane of the bacterium. Especially, the biosynthesis by *A. Xylinum* is controlled in association with a protein complex, as referred to "*terminal complex*" (TC) [1], which is arranged in a linear row on an outer membrane of the cell. Using UDP-glucose (Uridine disphosphate sugar), MC is synthesized as follows, UDP-glucose + $[\beta\text{-1,4-glucose}]_n \rightarrow$ UDP + $[\beta\text{-1,4-glucose}]_{n+1}$.

UDP-glucose has a molecular structure similar to adenosine triphosphate (ATP). From a point of view of materials science, the microbial film and its preparation are a new scientific topic of soft matter science, i.e., *reaction-induced self-assembly* in a non-equilibrium open system where physics, chemistry and biology crucially interplay.

To emphasize the peculiarity of MC, we examine a control system of synthetic polymer gel of poly(*N*-isopropylacrylamide) (PNIPAAm) [9], which is also swollen with a large amount of water (more than 93% by weight). It exhibits a lower critical solution temperature (LCST) for miscibility as for water. At the temperature T_V (≅ 33.5 °C), a PNIPAAm gel abruptly shrinks (collapsed phase), representing a first order phase transition (***volume phase transition***) [9]. Below T_V, the PNIPAAm gel is swollen with water (swollen phase). We examined self-assembled structure of these two hydrogels (MC and PNIPAM), in a wide range of length scales by using USANS and SANS. The scattering measurements on MC and PNIPAAm gel revealed that small-angle scattering obeys according to a power law *q*-behavior of $q^{-\alpha}$ as a function of a magnitude of scattering vector $\vec{q}$.

From the mass fractal *q*-behavior and its length scale limits, we evaluated a volume fraction of a primary unit. As a result of analyses, surprisingly found is that for MC, 90% of total water is trapped in a cellulose bundle giving local concentration fluctuations. Additionally, neutron diffraction elucidated that in the pellicle, the crystalline order is not developed. We concluded that a mechanism of excellent water-absorption of MC is capillarity due to hierarchically prepared non-crystalline structure, whereas for PNIPAAm gel, local hydration onto a monomer unit determines water-absorption. The length scales appearing non-crystalline structure are smaller than the length of bacterium at which we found the arrangement of TC in a linear row on an outer membrane of the cell.

2. Experimental

2.1. Preparation of microbial cellulose

A. xylinum, coded as ATCC strain 53582 (NQ-5), was cultivated in a Hestrin-Schramm (HS) culture medium (Ph = 6.0) of 200 cc, containing D-glucose, yeast extract and peptone (6, 1.5, 1.5, 0.35 and 1.53 g, respectively, in water 100 ml) [10]. After incubation of 2 weeks at 30 °C, we obtained a pellicle of 1 cm thickness, which is floating at air surface of HS culture medium (static cultivation). Pellicle was also by different cultivation conditions by shaking with different rational speeds (50 150 and 200 rpm, respectively).

To obtain pure MC without containing bacteria, we cut the pellicle at air side into a film specimen of 2–5 mm thickness. We examined two film specimens; (a) swollen by water and (b) dried completely. In order to obtain large scattering contrast, MC cultivated in the HS culture medium in H_2O, was first immersed in a large amount of D_2O over nights and H_2O was replaced with D_2O. A bulk concentration (ϕ_B) of MC is about 99% by weight. First, we examined the swollen MC by SANS and USANS. After the measurements, D_2O in the film specimen was completely removed in a vacuum oven. After drying, the height and width of the film specimen did not largely change (height and width = 40 × 30 mm^2). ϕ_B of dried cellulose was determined as 5.5 wt % by weight. For neutron diffraction measurements, we also caught a film from a bottom side of pallice in a culture solution.

2.2. Cultivation of bacterium

To obtain the bacterium for neutron scattering measurements, we prepared the two different HS culture mediums, together with protonated water (H_2O) (bacterium (H)) or deuterated water (D_2O) (bacterium (D)). In order to remove the produced cellulose, we added the degradation enzyme cellulase (ONOZUKA, R-10). After 350 h for (bacterium (D)) and 20 h for (bacterium (H)), we purified the culture solution and dried. The powders of bacterium were dissolved into a solvent of D_2O (1–3 wt %).

2.3. Preparation of PNIPA gel

A NIPAAm monomer (Kohjin Co. Ltd. Japan) was purified by recrystallizing its toluene solution in hexane at 4 °C. A pre-gel solution was prepared according to a recipe that NIPAAm monomer of 7.8 g, *N*, *N*-methylenebisacrylamide (BIS) of 0.345 g, and ammoniumpersulfate of 0.043 g are dissolved in D_2O of 100 ml. An initiator, N, N, N′, N′-tetramethylethylenediamine of 240 ml, was added to a pre-gel solution to initiate random copolymerization between NIPAAm and BIS (monomer-crosslinker). When monomer-crosslinking, the pre-gel solution was poured into a glass plate mold with a gap of 1.0 mm thickness. In order to obtain transparent and homogeneous gel, the temperature was kept at 10.0 °C, which is very far from volume phase transition (T_V = 34.0 °C). After polymerization, a NIPAAm film was immersed in excess amount of D_2O. water content was determined as 93.0 wt% by weight.

2.4. Neutron scattering

We employed two small-angle neutron scattering spectrometers at research reactor JRR-3, at Japan Atomic Energy Agency, Tokai, Japan. A focusing USANS spectrometer (SANS-J-II) was newly constructed using focusing compound lens (MgF_2) to cover a q-region of USANS ($10^{-4} < q < 0.003\,Å^{-1}$) [11–13], where q is defined as $q = 4\pi/\lambda sin$ (θ) with scattering angle 2θ and wave length λ. With neutron of $\lambda = 6\,Å$, SANS-J-II is able to choose conventional pinhole SANS collimations without a focusing setup, in order to cover $0.003 < q < 0.1\,Å^{-1}$ by changing two different sample to camera distance. In order to reach to the q-region of $10^{-5}Å^{-1}$order, we utilized double crystal (Bonse-Hart) USANS spectrometer (PNO) at JRR3, Tokai [14]. By using grooved perfect silicon crystals and thermal neutron of $\lambda = 2\,Å$, we can cover from $q = 3 \times 10^{-5}$ to $10^{-4}\,Å^{-1}$.

In order to determine crystalline structure in a pellicle and dried MC, we utilized a triple axis spectrometer (TAS-1) at JRR-3 with a polarized neutron beam [15]. The method of polarization analysis allows us to quantitatively discriminate coherent scattering from the crystalline structure and incoherent scattering from hydrogen. The detail of USANS and polarization analysis are summarized in Appendix.

3. Experimental results and discussion

3.1. Macroscopic observation

Fig. 2 shows the pellicle obtained by different cultivation conditions. With a static condition (see Fig. 2 (a)), a pellicle film is flat and floats at the top of culture medium. By shaking with different rational speeds (Fig. 2 (b) 50 (c) 150 and (d) 200 rpm, respectively), the pellicles were layered, balled and powdered, respectively. Within a variety of the pellicles depending on the culture conditions, next, we focus on the pellicle with a static cultivation condition.

Fig. 3a shows the pellicle obtained with a static cultivation condition after several days. At the air side, the pellicle is stiff and more turbid, while at the liquid side, it is more swollen by the solution showing a jelly form. It is possible that the during the cultivation, water is evaporated from the surface at air. Later in sec. IV-2-3, the pellicle obtained from the liquid side is examined by neutron diffraction to determine crystalline order during cultivation. Fig. 3b shows the pellicle obtained after 2 weeks. It is marvelously swollen by water, the water content of which is about 99% by weight. As shown in Fig. 3b, it is strongly turbid, indicating inhomogeneity in concentration on mesoscopic length scales. Water is easily squeezed by compression with a finger.

Fig. 4a shows a block of PNIPAAm gel swollen with water. Even with a large water content about 93 wt%, it is transparent. We stress that water can not be squeezed by compressing. Even after smashing

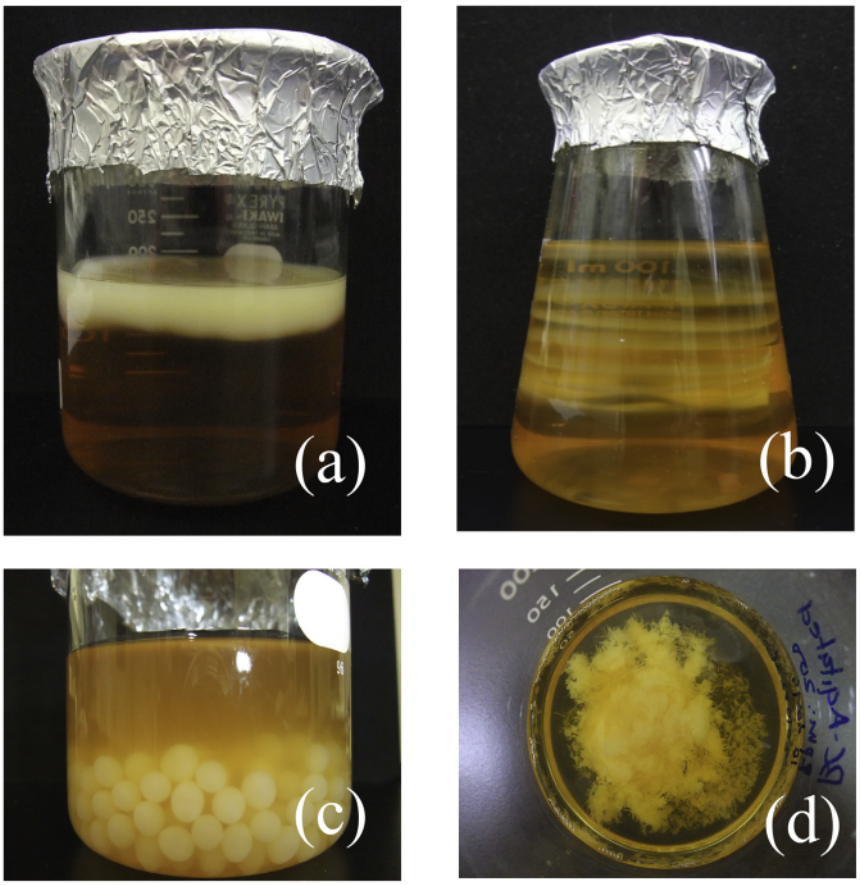

Fig. 2. Photos of pellicle obtained by different cultivation conditions of (a) a static condition, and with different rational speeds (b) 50 (c) 150 and (d) 200 rpm, respectively.

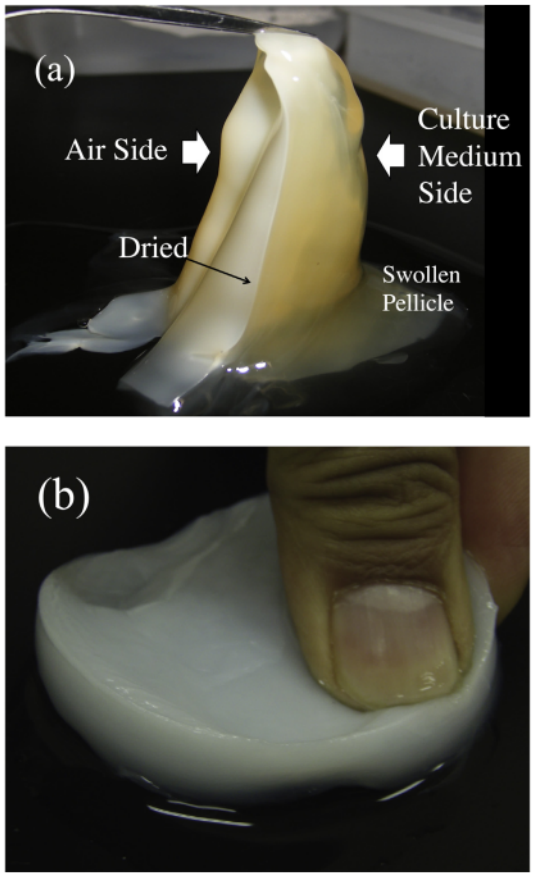

Fig. 3. (a) Photo of fresh pellicle, picked up from the culture medium. (b) Photo of microbial cellulose after 2 weeks of cultivation. It is swollen by water (99% by weight) and water is squeezed by compression with a finger.

the gel (Fig.4b), PNIPAAm gel never releases water at room temperature about 20 °C, which is far below LCST in a swollen state.

3.2. Neutron scattering

3.2.1. Bacterium body

Fig. 5a shows the results of SANS and USANS for the acetic bacteria. The wide q-region is covered by double crystal USANS, focusing USANS and pinhole-type SANS (camera distance 10 m or 2.5 m). In the q-range of USANS ($q < 0.001$ Å^{-1}), scattering intensity changes according to q^{-1}. Meanwhile, at larger q (> 0.001 Å^{-1}), scattering intensity changes according to q^{-4}. A difference between the cultivations in H_2O and D_2O starts from $q = 0.01$ Å^{-1}, which is attributed to the local structure of the bacterium, such as cytoplasm, cell wall and TC allocated on the body. In Fig. 5a, the length scales L_1 -L_4 are indicated; L_1 and L_2 correspond to pore and whole sizes of TC, while L_3 and L_4 are diameter and major axis length of the bacterium.

3.2.2. Swollen and dried MC

For swollen MC (open squares in Fig. 5b), we find characteristic q-behaviors according to power laws $\sim q^{-\alpha}$. From higher q values, found are $\alpha = 2.35$, $\alpha = 1$ and $\alpha = 2.5$ for $0.001 < q < 0.1$, $0.0003 < q < 0.001$, $0.00003 < q < 0.0003$ Å^{-1}, respectively. The upper and lower limits for these are denoted as q_1, q_2, q_3 and q_4, respectively in Fig. 5b. At q_2, there is a hump, deviating from the power laws.

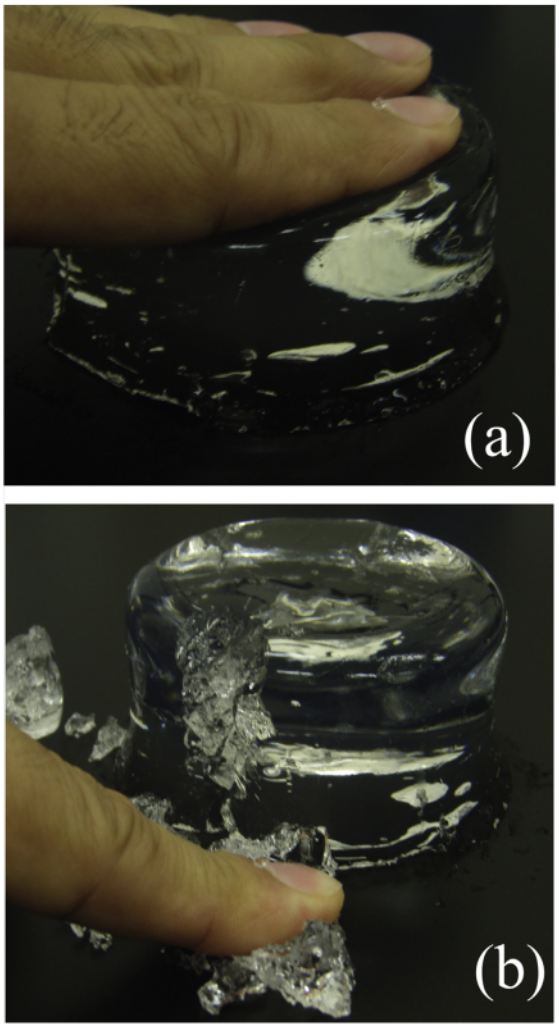

Fig. 4. Photo of PNIPAAm gel swollen with water (water content about 93 wt %). (a) Water is not squeezed by compressing, and (b) a gel swollen with water is powdered by pressing.

The power law q-behaviors were strongly affected by drying, as indicated by filled circles in Fig. 5b. By searching from higher q values, we found $\alpha = 4$, $\alpha = 2.4$ and $\alpha = 2.5$ for $0.001 < q < 0.005$ Å^{-1}, $0.005 < q < 0.07$, $0.00003 < q < 0.0008$ Å^{-1}, respectively. We denoted the upper and lower limits for the power laws as q_5, and q_6, as shown in Fig. 5b.

3.2.3. Crystalline structure of MC

Fig. 6 shows the scattering profiles obtained by a triple axis spectrometer (TAS-1). The SANS profiles, which are shown in Fig. 5b, are plotted together. For the as-prepared pellicle (Fig. 6a), it was found that diffuse scattering from amorphous cellulose dominantly appears with small diffraction maxima originating from crystalline structure. It should be emphasized that after polarization analysis, the scattering profile is a coherent and elastic scattering function $S(q,\omega = 0)$. After drying (Fig. 6b), we start to observe the scattering maxima due to crystalline order of cellulose chains. After heat treatment with pressing (Fig. 6c), the crystalline order is more developed. The 1st, 2nd and 3rd

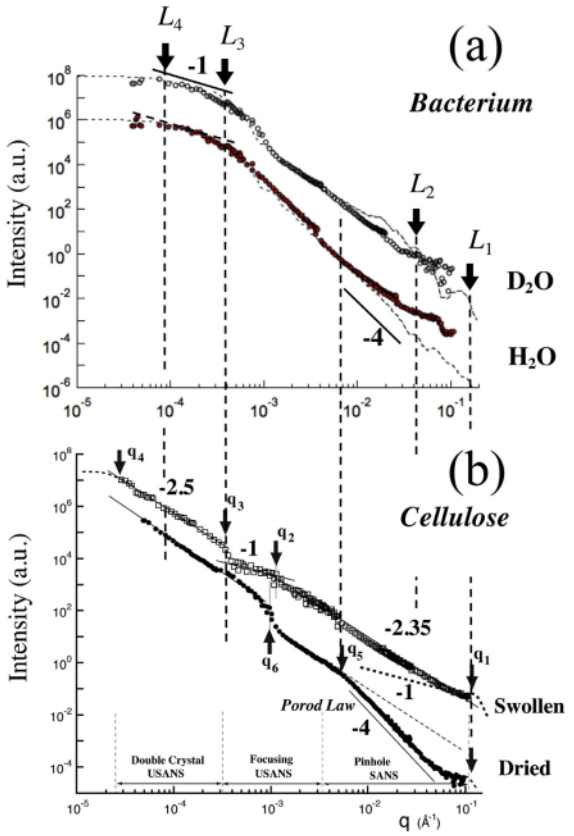

Fig. 5. (a) SANS and USANS profiles obtained for the bacterial cell, *Acetobactor Xylinum*, cultivated in culture mediums containing H_2O and D_2O. Characteristic lengths related to cell body (L_1, L_2, L_3 and L_4, respectively) are indicated. Broken lines are calculated by a holo-cylinder model, considering scattering contrast Δb_1 and Δb_2, respectively. (b) SANS and USANS profiles obtained for the pellicle swollen with D_2O and the dried pellicle. USANS changes in accordance with an exponential function ($q^{-\alpha}$). Crossover q for different power law α is indicated q_i (i = 1–6).

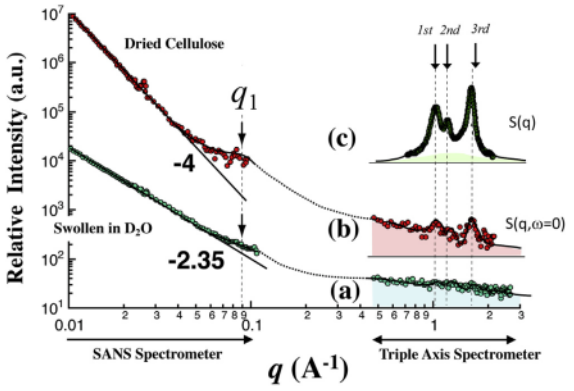

Fig. 6. Coherent scattering profiles obtained by a triple axis spectrometer (TAS-1). For (a) the as-prepared pellicle, (b) after drying and (c) after pressing the film with heat.

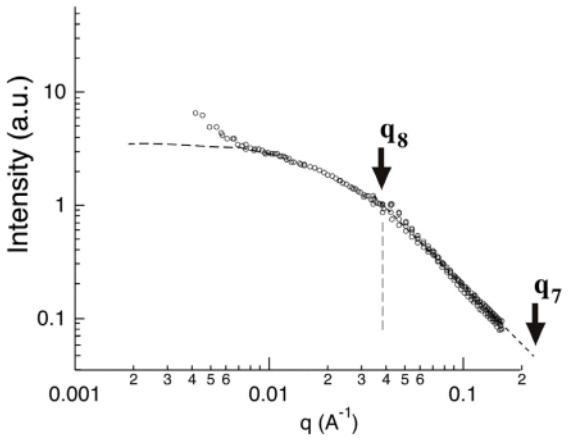

Fig. 7. SANS profile obtained for the PNIPAAm gel at 28 °C. q_7 and q_8 denote the q-limitations of mass fractal behavior of $\alpha = 1.67$.

maxima (Cellulose I) are attributed to (101), (10$\bar{1}$) and (002).

We evaluate the width of scattering maximum quantitatively with a Scherrer's equation [16], and the size of crystallite (L) is determined given by,

$$L = 0.9\lambda/d\theta\cos\theta, \quad (1)$$

where $d\theta$ denotes a width of scattering maximum. For the TAS measurements with $\lambda = 2.359$ A, we observed the most prominent diffraction (002) at $\theta = 17.5$ deg with $d\theta = 0.6$ deg (the corresponding q is $q = 1.60$ A^{-1}). From the width of scattering maximum, we evaluated the size of crystallite as $L = 7$ nm ($= R_1$), which corresponds to the position of q_1 ($= 2\pi/R_1$).

3.2.4. PNIPAAm gel

Fig. 7 shows a SANS q-profile obtained for the PNIPAAm gel at 28 °C. The q-profile of the swollen PNIPAAm gel exhibits similar to that given by the Ornstein-Zernike formalism. Following a scheme of the blob, we found power law scattering of $q^{-\alpha}$ at higher q, due to mass fractal of monomer distribution in water. In Fig. 7, q_7 denotes a wave number given by a monomer size ζ ($q_7 = 2\pi/\zeta$ where $\zeta = 1$ nm). From the higher q-region of $q > 1/\xi$, we determined $\alpha = 1.67$ close to the Flory exponent, indicating water behaves as a good solvent at 28.0 °C. A deviation from the power law occurs at $q_8 = 1/\xi$, where ξ is the screening length or blob size in a swollen gel.

4. Discussion

4.1. Hierarchy in bacterium body

Fig. 8 (a) shows a schematic view of bacterium body, which is illustrated on a basis of the TEM observation shown in Fig. 1. The bacterium body is further approximated by a holo-cylinder structure (or two-fold cylinder) in Fig. 8 (b), where the shell and core parts correspond to the cell wall and cytoplasm. The length of bacterium is indicated by $2H$ ($= L_4$). The radius of outer and inner cylinders is given by D_1 and D_2, respectively. Note that $2D_1 = L_3$. The contrast (difference in scattering length density) for the cytoplasm and cell wall are indicated by Δb_1 and Δb_2. The core of bacterial cells cultivated in the H_2O was filled with H_2O and had bulk contrast ($\Delta b_1 = \Delta b_2 \neq 0$ in Fig. 8 (b)). Meanwhile, the core and outer shell of the cell cultivated in the D_2O were filled with D_2O and had a contrast whereby the cellular membrane stood out (film contrast) ($\Delta b_1 \neq 0$, $\Delta b_2 = 0$ in Fig. 8 (b)).

Next, we evaluate small-angle scattering from the bacterium using a model of two-fold cylinder [17]. A scattering amplitude for the holo-

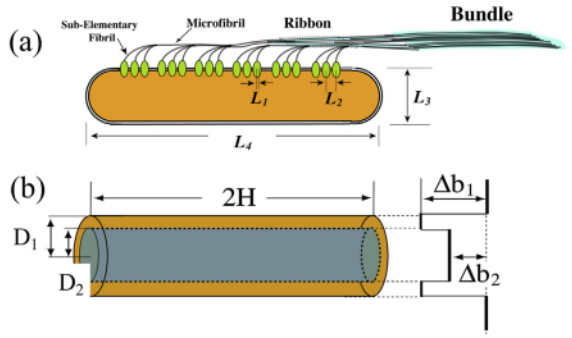

Fig. 8. (a) Schematic diagram of bacterium body and microbial cellulose, which is illustrated on a basis of TEM in Fig. 1. The size and distance of TC are L_1 and L_2, respectively. The diameter and length of bacterium are L_3 and L_4, respectively. (b) Bacterium body is approximated by a holo-cylinder structure (outer and inner radius D_1 and D_2, respectively and the length is 2H), where shell and core correspond to the cell wall and cytoplasm with scattering contrasts (Δb_1 and Δb_2, respectively).

cylinder structure is given by,

$$F(q,\alpha) = 2\Delta b_1 v_1 \frac{\sin(qH\cos\Phi)J_1(qD_1\sin\Phi)}{(qH\cos\Phi)(qD_1\sin\Phi)} + 2\Delta b_2 v_2 \frac{\sin(qH\cos\Phi)J_1(qD_2\sin\Phi)}{(qH\cos\Phi)(qD_2\sin\Phi)} \quad (2)$$

where Φ is an angle between scattering vector and major axis of cylinder. The parameters v_1 *and* v_2 are specific volume for cytoplasm and cell wall ($v_1 = v_2 = 1$). The thickness of cell wall ΔD is given by

$$\Delta D = D_1 - D_2 \quad (3)$$

With eq. (2), SANS intensity for the randomly orientated bacterium is given by

$$I(q) = \frac{N}{V_r}\int_0^{2\pi} F(q,\Phi)^2 \sin\Phi d\Phi \quad (4)$$

In eq. (4), N and V_r are the number of cylinders and a volume of a cylinder. The contrasts, Δb_1 and Δb_2, are

$$\Delta b_1 = b_{D2O} - b_M,\ \Delta b_2 = b_{D2O} - b_C(\varphi) \quad (5)$$

and

$$b_C(\varphi) = \varphi b_{water} + (1-\varphi)b_{pro} \quad (6)$$

b_{water} corresponds to b_{H2O} or b_{D2O}, depending on the cultivation conditions. In the cytoplasm, we find a variety of organic molecules such as proteins, polypeptides, nucleic acid (DNA and RNA) and lipids. In our model, the scattering length density for the cytoplasm b_C is replaced with a mixture with a representative protein, Lysozyme, and water. A mixing ratio is given by φ (volume fraction of water) in eq. (6). The core is composed of organic molecules and water, whose scattering length density are b_{pro}, b_{H2O} or b_{D2O}, (= 3.5×10^{10}, -0.5×10^{10} and 6.4×10^{10} cm^{-2}, respectively). The cell wall, on the other hand, is composed of double membranes of poly peptidoglycan and plasm membrane with a gap of periplasmic space. In our model, we assume the wall is uniform whose scattering length density is given by $b_M = 0.4 \times 10^{10}$ cm^{-2}.

Using the equations of (2)–(6), we evaluate the scattering q-profiles for the bacterium (dotted line, Fig. 5a). From the electron microscopy, we determined as $2H = 10\,\mu m$, $D_1 = 1\,\mu m$, and the form factor of randomly-oriented two-fold cylinder was calculated with $\Delta D = D_1 - D_2 = 10\,nm$. From the scattering contrast Δb_2, we determined a water content φ = 0.66 in eq. (6), which is reasonably agrees with the knowledge in Ref. [18].

We found that the evaluated q-profiles agree well with the experiments in the range of $q < 5 \times 10^{-3}$ Å^{-1}. In the lowest q, the scattering follows Guinier's law and the radius of gyration R_g of the bacterial cell is given by,

$$R_g = [({D_1}^2/2) + (H^2/3)]^{1/2}. \quad (7)$$

Moreover, in the q-range between the two arrow marks, the decay of the scattering intensity is in accordance with q^{-1}, and the location of the arrow marks corresponds to the diameter (L_3) and the major axis length (L_4) of the bacterial cell. The significance of q^{-1} is that a bacterial cell appears as a long and narrow cylinder on this length scale. Meanwhile, the evaluated curves and experimental results do not agree at $10^{-2} > q > 10^{-1}$ Å^{-1}, but this is possibly because the microstructures of TC's and other aspects of bacterial cells such as cell walls were not taken into the calculations in the two-fold cylinder model used here. However, even with an analysis as simple as this one, the approximate information for the bacterial cell can be acquired in the lower q-region.

4.2. Hierarchy in MC

For USANS and SANS obtained for MC and PNIPAAm gel, we found q-behaviors according to power law of $q^{-\alpha}$, with α varying between 1 and 3. We attribute the power laws between 1 and 3 to mass fractal for a spatial distribution of a primary mass unit [17,19]. For MC, a unit is a crystallite (microfibril), whereas for a PNIPAAm gel, it is a monomer unit. Note that the surface fractal dimension d_s in the relationship of $\alpha = 6 - d_s$ varies from 2 to 4 and that Porod's law is equivalent to a surface fractal dimension $d_s = 2$.

According to a scheme of mass fractal, total mass $M(R)$, occupying a space of volume R^3, changes as R increases, given by

$$M(R) \sim R^{dm}\ (1 < d_m < 3), \quad (8)$$

where d_m is identical to a power law exponent α, which is determined by a small-angle scattering technique. The fractal behavior is limited by upper and lower length scale limits (R_L and R_U). By the scattering method, we can determine the limits as wave numbers q. Note that these limits are given by $R_L = 2\pi/q_L$ and $R_U = 2\pi/q_U$.

Fig. 9 summarizes the fractal dimensions for the swollen and dried MC. Note that $R_i = 2\pi/q_i$, for i = 1–7. For the swollen MC (see Fig. 9a), $\alpha = 2.5$ in the lowest q-region is due to a network structure composed of bundles, which appears on length scales from 1 to 20 μm $\alpha = 2.35$, found in the highest q, is attributed to the concentration fluctuations in the bundle composed of crystallite and non-crystalline cellulose swollen with water. The power law of $\alpha = 2.35$ is limited at q_1 (= 0.07 Å^{-1}), which is equivalent to $R_1 = 7$ nm (=$2\pi/q_1$). By TAS-1 with polarization analysis, on the other hand, the size of crystallite was experimentally determined as L or $R_1 = 7$ nm (=$2\pi/q_1$), which is equal to the size of

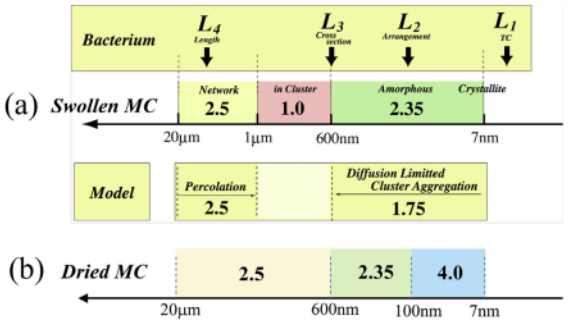

Fig. 9. Summary the mass fractal dimensions determined by USANS and SANS for (a) swollen MC and fractal model and (b) dried MC. The length scales of upper and lower limitations are determined by q-limitations (~$2\pi/q$).

crystallite (microfibril). We attribute $\alpha = 1$ found in the middle q-region ($q_3 > q > q_2$) to a bundle structure (one-dimensional and rod-like shape), composed of the cellulose swollen with water. q_2, upper q-limit for $\alpha = 1$, indicates a cross-section size of the bundle, which was evaluated as $R_2 = 600$ nm ($=2\pi/q_2$).

For the dried MC, $\alpha = 4.0$ for $R < R_5 = 100$ nm ($=2\pi/q_5$) is attributed to a Porod law arising from a sharp interface between *cellulose ribbon* (matrix is air). The size $R_5 = 100$ nm is close to the width of cellulose ribbon reported in Fig. 3 of ref.2. The power law $\alpha = 2.35$ appears from 600 to 125 nm, while $\alpha = 2.5$ for the network appears from $R_6 = 600$ nm.

4.3. Fractal analysis

By combining with mass fractal dimension d_m and upper and lower length scale limits (R_L and R_U), we evaluate a volume fraction of cellulose $\phi(R)$, by simply normalizing $M(R)$ with R^3. Therefore, $\phi(R)$ is as,

$$\phi(R) = \left(\frac{R}{R_L}\right)^{-(3-d_m)} \quad \text{for } R_L < R < R_U \tag{9}$$

According to eq. (9), $\phi(R)$ varies, when we change a length scale of observation R. Finally when R increases largely enough, $\phi(R)$ reaches to bulk concentration ϕ_B, which is independent of R.

In Fig. 10, ϕ(R) is shown for the swollen and dried MC. For the swollen MC ((a) in Fig. 10), from at R_1(=7 nm), $\phi(R)$ starts to decrease according to $R^{-0.65}$. Note that the power of 0.65 was obtained from 3-α with $\alpha = 2.35$. At R_2 (=600 nm), the slope of $\phi(R)$ changes to 2 due to $\alpha = 1.0$ for the bundle structure. For $R_3 < R < R_4$, the slope of $\phi(R)$ is 0.5 due to $\alpha = 2.5$ for the network structure. Finally at $R_4 = 20$ μm, $\phi(R)$ reaches to 0.01, which is equivalent to ϕ_B, determined by weight.

For the dried MC ((b) in Fig. 10), $\phi(R)$ indicates the volume fraction of cellulose ribbon. Therefore, $\phi(R)$ starts to decrease from the ribbon size R_6 (=125 nm) according to $R^{-0.65}$. For $R_6 < R < R_7$, $\phi(R)$ obeys $R^{-0.5}$. Finally, at R_4 (=20 μm), $\phi(R)$ reaches 0.08, which is close to $\phi_B = 0.055$, which is the weight fraction of the dried MC.

$\phi(R)$ for the swollen PNIPAAm gel was also evaluated ((c) in Fig. 10). $\phi(R)$ is a fraction of NIPAAm monomer in a swollen state. $\phi(R)$ for the PNIPAAm gel starts to decrease from a monomer size R_7 (=1 nm) according to $R^{-1.33}$. At $R_8 = 16$ nm, corresponding to a correlation length of the concentration fluctuations in the gel, $\phi(R)$ reaches to ϕ_B of about 0.02. Beyond this length scale, $\phi(R)$ does not depend on R.

Both of hydrogels PNIPAAm and MC are swollen by a large amount of water more than 90% in weight. However, Fig. 10 visualizes that water is stored in different ways. $\phi(R)$ for PNIPAm gel decreases to 2–3% within a length scale domain from 1 nm to R_8. Meanwhile, $\phi(R)$ for MC decreases to 1% within a length scale domain from 10 nm to 10 μm. The length R_4 and R_8, at which $\phi(R)$ reaches to ϕ_B, are so different (see the arrows shown in Fig. 10).

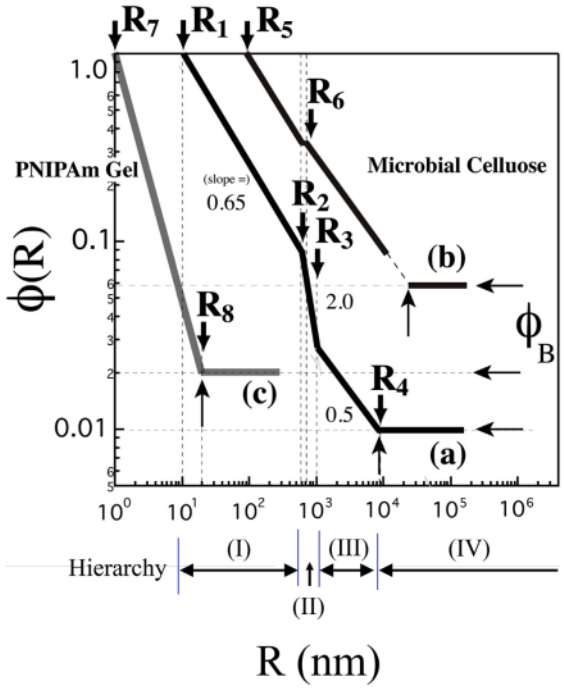

Fig. 10. Volume fraction of microbial cellulose in water $\phi(R)$ evaluated for (a) swollen and (b) dried cellulose, by mass fractal analysis based on eq. (37). R_1 (=7 nm) corresponds to a size of microfibril.

4.4. Mechanism of water uptake

By compressing with a finger, MC easily squeezes water to outside, as shown in Fig. 3b. Meanwhile, the PNIPAAm gel in Fig. 4 never squeezes water in a swollen state below a LCST line. The excellent capability of water uptake found for MC is attributed to "***capillarity***". Occurs "*impregnation*" or "*intercalation*" of water molecules into noncrytstalline domains in MC. According to the literature [20], the capillarity pressure for absorption ΔP is inversely proportional to a pore size R_p,

$$\Delta P \sim \Delta\gamma / R_p, \tag{10}$$

where $\Delta\gamma$ is difference in surface tension between wetting and dewetting states. We suppose that the pore in MC varies according to the mass fractal behavior as determined by SANS and USANS. A positive sign of $\Delta\gamma$ indicates affinity of water impregnation into MC. The smaller pores contribute more to absorb water effectively. In the case of microbial cellulose, we study, the pore appears according to a mass fractal law of eq. (8) with $d_m = 2.35$. The fraction of pore is given by 1-ϕ(R) and eq. (9).

To the contrary, the PNIPAAm gel tightly binds water molecules by means of ***hydration*** at a hydrophilic amide group. Therefore, it never releases water by compression. The macroscopic swelling behavior of the PNIPAAm gel was examined by Flory interaction parameter χ ($\sim \Delta H/T - \Delta S$) was determined as ΔH and ΔS = -130±50×10^{-15} erg and $-4.5\pm1\times10^{-16}$ erg/K, respectively [21]. Due to a large negative value of ΔH, which is attributed to strong binding of water molecules to an amide group, the NIPAAm gel never squeezes water below T_V (=34 °C), as shown in Fig. 4. A negative value of ΔS due to ordering of water molecules around NIPAAm side chains, is responsible for LCST, which is referred to *hydrophobic effect* [21].

Related to the strong local hydration, a peculiar phase behavior was reported for PNIPAm solutions (including PNIPAm gel). A LCST line is very ***"flat"*** [22] independent of both polymer concentration and molecular weights of PNIPAM, as referred to "miscibility square". In addition to a delicate balance between hydrophilic and hydrophobic groups, *"sequential cooperativity in hydration along a single chain"* (referred as to ***cooperative hydration***) which is crucial in order to reproduce the peculiar phase behaviors found for PNIPAm solutions [23].

4.5. Interplay among physics, chemistry and biology

What are the factors to determine the hierarchical structure of MC and its marvelous water uptake? To address the question, we performed USANS and SANS measurements on both of the bacterium and microbial cellulose and evaluated the scattering on the basis of a scheme of mass fractal (materials science). It is understood as the interplay among

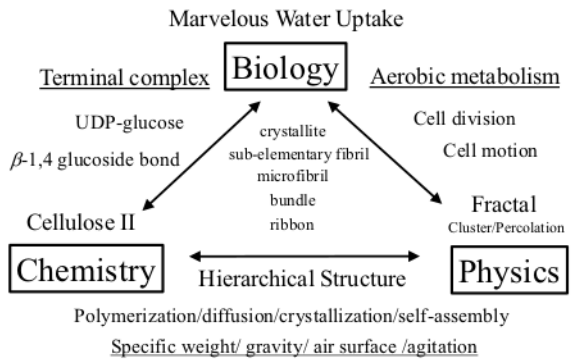

Fig. 11. Schematic diagram indicating the interplay among physics, chemistry and biology for microbial cellulose.

physics, chemistry and biology, which is illustrated in Fig. 11.

For the biological points of view, we find a strong relation between bio-synthesis and "*terminal complex*" (TC). MC is synthesized by the bacterium using the reactant UDP-Glucose, making β-1.4 Glucoside bond. The polarity of cellulose chains is parallel (as referred to Cellulose I). This is because the biosynthesis of MC is controlled in association with TC, which is arranged in a linear row on an outer membrane of the cell. The individual cellulose chains can not turn each other to form anti-parallel.

A cell motion, and cell division, also affect the hierarchy we expect. To visualize this situation, we introduced a key structure of "***cluster***" domain in Ref. [2]. In the cluster, the individual bacteria coherently (parallel) move due to chain constraint and cellulose chains are aligned parallel (see Fig. 5: in Ref. [2]). The cluster size should be close to the size of bacterium body (L_3 and L_4). The mass density of MC is smaller than the culture medium solution. Therefore, a pellicle is floating on the top of air surface (effect by gravity). The air surface is rich in O_2 so that the cell motion should be parallel to the surface. Cell division causes to split of the cluster domain.

Related to the mass fractal dimensions determined by SANS and USANS, we classify the structural hierarchy (I), (II), (III) and (IV).

4.5.1. Structural hierarchy (I) and (II)

The formation of hierarchical structure of the pellicle is initiated by a nearly simultaneous and subsequent physicochemical processes of polymerization, crystallization and molecular assembly, which occur in or in the vicinity of the cell membrane of the bacterium. *A. Xylinum* with TC's on the body is a weaving machine, making cellulose ribbon, micro-fibril and sub-elementary fibril and crystallite. It weaves cellulose chains and water together. Consequently, the cellulose chains are prevented from crystallization. Surprisingly, 90% of total water is accumulated in the cellulose bundle, which appears in a cluster domain.

For the length scales smaller than a cluster size, we determined $d_m = 2.35$, which is related to a model of diffusion limited cluster aggregation (DLCA) [24] with indicating $d_m = 1.75$ for a spherically symmetric primary particle. It should be reminded that MC is composed of a one-dimensional primary unit, such as a microfibril. For a direction parallel to the major axis (z-axis), the mass fractal dimension is $d_{mz} = 1$. If we postulate that the mass is equally distributed in x-y plane, we obtain $d_{my} = d_{mz} = 0.67$ (= (2.35–1)/2). Nota that for a common DLCA model, the mass is distributed equally in x, y and z directions, so that we obtain $d_{mx} = d_{yx} = d_{mz} = 0.58$ (=1.75/3). The value of d_m we found in x-y plane found for MC is slightly larger than that of DLCA. This is possibly because the cellulose chains are extruded from adjacent TCs and aggregate side by side. Consequently, the packing of cellulose chains is denser than the case of common DLCA. A rigid cellulose chain is characterized by "***an-isotropic excluded volume interaction***", which affects its association. It should be denoted that d_m larger than 0.58 is widely found for the systems with an isotropic excluded volume interaction, such as actin bundle formation [25] and colloidal rod aggregation (boehmite) [26].

4.5.2. Structural hierarchy (III)

The network, which results in $d_m = 2.5$ for larger length scales of μm should result in the ***cluster-cluster aggregation***. The cluster size is comparable to the seizes of the bacterium (L_4 and L_3) are ~10 μm and 1.0 μm, respectively.

4.5.3. Structural hierarchy (IV)

The volume fraction $\phi(R)$ is equal to ϕ_B in this region. The macroscopic shape of pellicle film is determined by an agitation condition.

4.6. Perspective. Materials Science, Artificial synthesis of polymers

In addition to the microbial cellulose [2–6], the artificial synthesis of cellulose by enzymatic catalysis [27–29] was also investigated. We extended our investigations to self-assembly induced by chemical reaction, which is a "open" and non-equilibrium system. When we observe the structural formation that takes place in the natural world, as seen in the example of cellulose, as important point is that self-organization occurs continuously and immediately next to the synthesis reaction.

Because of our interest in ordering in nature, we aimed to perform in situ observation in the reaction medium by using SANS. We examined the reaction solutions of living anionic polymerization [30–33], living radical polymerization [34,35], solid-phase or soap-free radical polymerization by radiation processes [36,37], oxidation-reduction reaction of metal nano-particle formation [38-41],. The computer simulation was performed to reproduce self-assembly in the reaction solution [42,43]. These are a new scientific topic of soft matter science, i.e., *reaction-induced self-assembly* in a non-equilibrium open system where physics, chemistry and biology crucially interplay.

Fig. 12 shows a photo of the reactor cuvette for pre-irradiation radical polymerization making grafted film. As the name implies, neutron is electrically neutral. The excellent transmissivity of neutron through matter is also of significant value. Therefore, we are able to prepare a sample cuvette for reaction solution as large as that the researcher usually use in a chemistry laboratory. Neutron has the properties of having mass and low energy (around several meV). Because of these, breaking of chemical bonds and formation of radicals do not occur under neutron irradiation. In other words, in environments where materials and organisms exist, their structure can be observed in situ by using the unique contrast afforded by neutrons. Neutron is a marvelous probe to see the living system as it exists.

5. Conclusion

We examined the hierarchical structure in the microbial cellulose and a bacterium body over a wide length scales from 1 nm to 10 μm. By using ultra-small-angle & small-angle neutron scattering techniques, the hierarchy in structure is characterized by a mass fractal scheme. The mass fractal dimensions are determined, depending on the length-scale of observation. According to quantitative analyses based on mass fractal and its length scale limits, it was elucidated that 90% of water is stored in non-crystalline bundle structure. The formation of MC is tightly related to the local structures in a bacterium body. Non-crystalline order in as-prepared MC was examined by neutron diffraction by a triple-axis spectrometer with polarization analysis. With these structural informations, we conclude that the absorption mechanism of MC is capillarity, whereas that for the synthetic polymer gel of poly(*N*-isopropylacrylamide), is the tight hydration onto a monomer unit via a hydrogen bond.

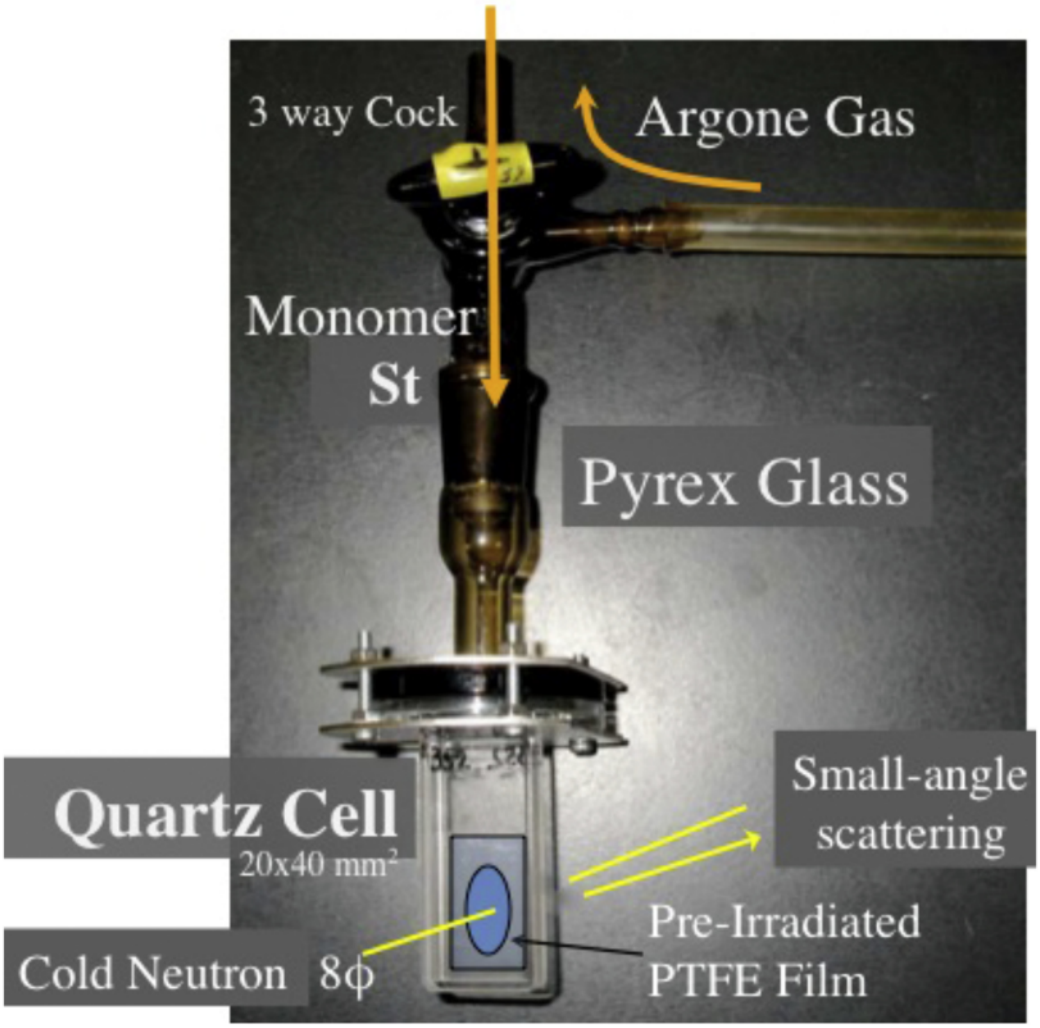

Fig. 12. Photo of reaction cuvette for in-situ observation of living polymerization (pre-irradiation radical polymerization).

Acknowledgements

Part of works discussed in this paper has been performed as a research activities in the research group of soft matter at Advanced Research Center of JAEA (from 1997 to 2006), the group leader of which was Prof. Takeji Hashimoto.

Appendix

Advanced Small-angle Neutron Scattering

The technique and spectrometer of neutron scattering were developed by considering a variety of fundamental properties of neutron [44]. To extend the q-region toward smaller or larger using a monochromatic beam, at research reactor JRR3M, Tokai Japan, focusing neutron lens was employed and installed on the conventional SANS instrument SANS-J at JRR3, Tokai, Japan [11–15]. The intensity of small-angle scattering $I(q)$, obtained as a function of q, is related to differential scattering cross section $\frac{d\Sigma}{d\Omega}(q)$, which is defined as scattered neutron into a solid angle window $\Delta\Omega$. $\frac{d\Sigma}{d\Omega}(q)$ includes the structural information in reciprocal space, which is a Fourier transform of the microstructure in real space [45]. To obtain $I(q)$, it is further multiplied by incident beam flux I_0, which are determined by a source and scattering spectrometer we choose, sample cross section and thickness (A_S and D_S) and transmission T_s,

$$I(q) = K_I I_0 (A_s D_s) T_s \frac{d\Sigma}{d\Omega}(q)\Delta\Omega \tag{A1}$$

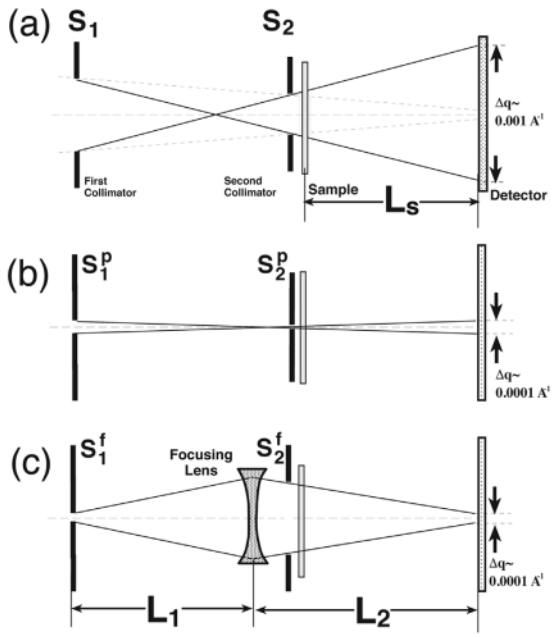

Fig. 13. Schematic diagram of pinholes for SANS instruments for (a) conventional SANS, (b) brute force methods by narrowing the pinholes and (c) focusing USANS with lens.

K_I is an instrument constant. We define a wave number q, as follows

$$q = 4\pi / \lambda \sin(\theta) \ , \tag{A2}$$

where λ and 2θ are wave length and scattering angle, respectively. The observation length Λ is related to $\Lambda = 2\pi/q$. By using the distance from the sample to the detector (L_S) and spot size (P) at the detector, the angular resolution $\Delta\theta$ can be formulated as

$$\Delta\theta \cong P/L_s \tag{A3}$$

In general, $q_{\min}$ is an index that denotes the performance of the small-angle scattering apparatus and is given by

$$q_{\min} = 2\pi \ \Delta\theta \ /\lambda. \tag{A4}$$

Thus, from (A-3) and (A-4), we have

$$q_{\min} = 2\pi(P \ /\lambda L_s). \tag{A5}$$

Experimentally, $\Delta\theta$ is given by scattering geometry with the pinhole sizes (S_1^P and S_2^P). After a sample position, incident neutrons of radius R arrives at the detector.

Fig. 13a shows the collimation for conventional SANS instruments [46,47] with pinhole size (S_1^P and S_2^P) and the detector distance (L_s) has the advantage of facilitating the adjustment of $\Delta\theta$ of the incident neutrons and the optimization of the resolution (i.e., $q_{\min}/q$ is usually of the order of 0.1).

Toward ultra-small-angle scattering, we narrow S_1^P and S_2^P (typically 2 and 1 mm, respectively) to obtain smaller $\Delta\theta$ (***brute force method,*** see in Fig. 13b). However, we encounter fatal loss of sample volume ($A_S \ D_S$) irradiated by incident beam, which is a problem for neutron scattering with a smaller flux.

The idea to overcome the loss is to use of focusing lens [11–13,48,49], which is allocated at a sample position (***focusing method,*** see in Fig. 13c). The lens focuses the incident beam and reproduces the beam size as large as the slit at upper stream (S_1^f), whereas the beam size at a lens is S_2^f. Pin holes for focusing SANS are S_1^f and S_2^f (typically 2 and 20 mm, respectively). We define a gain factor for focusing, as follows,

$$G = \left(\frac{S_1^f \ S_2^f}{S_1^P \ S_2^P}\right)^2 T_R^{lens} \tag{A6}$$

where T_R^{lens} is transmission for lens itself. $T_R^{lens}(=0.5\ )$ was determined for the MgF_2 crystal lens which was installed on SANS-J-II spectrometer at JRR3. We obtain a gain $G = 200$, with a combination of S_1^P and S_2^P ($=$ 2 and 1 mm) and S_1^f and S_2^f ($=$ 2 and 20 mm), respectively. A variety of focusing lenses is available for ultra-small-angle scattering, using refractive material lens [50–52] and magnetic lens [53]. Similarly, there are methods for beam focusing with a single crystal [54] multi-pinholes [55] and reflection mirror [56]. Lamor precession is also available to achieve USANS [57].

For double crystal USANS (Bose-Hart type geometry [58,59]), $\Delta\theta$ (denoted as $\Delta\theta_D$) is given by Ref. [60].

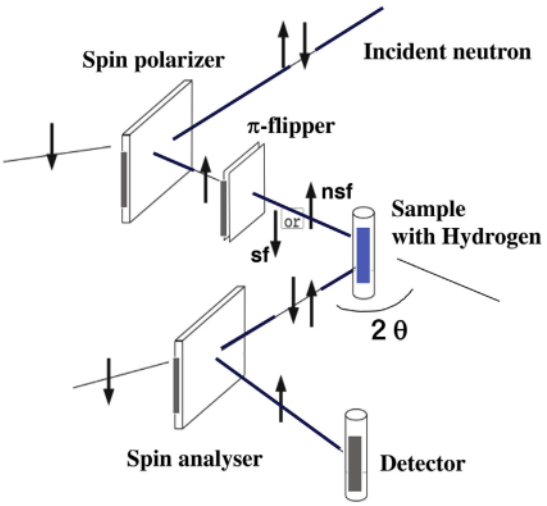

Fig. 14. Schematic diagram of polarization analysis with spin polarizer, π-flipper and spin analyzer.

$$\Delta\theta_D = \left(\frac{\lambda_{hkl}^2}{\sin(2\theta_B)}\right) \times \left(\exp\left(-M\right) \times \frac{b_c|F_{hkl}|}{\pi V_c}\right) \tag{A7}$$

where λ_{hkl} $(=2d_{hkl}\sin\theta_B)$ is wave length of Bragg diffraction. F_{hkl} is crystal structure factor, b_c is coherent scattering length, V_c is a volume of unit cell. The exponential function is Debye-Waller factor given by

$$M = 8\pi^2 < u^2 > \left(\frac{\sin\theta_B}{\lambda_{hkl}}\right) \tag{A8}$$

$< u^2 >$ is a mean squared displacement along a direction of reflection plane. Note that $< u^2 > = 0.45\,A^2$ for a silicon crystal. For the double crystal method, q_{min} is determined by eq.(A-4) and (A-7). In other words, q_{min} is determined by the quality of crystal itself which is described in a second term of (A-7). q_{min} is not related to the distance L_s different from pin-hole type SANS. It should be stressed that $\Delta\theta_D$ is proportional to λ^2. With a shorter wavelength, we are able to achieve smaller $\Delta\theta_D$ and q_{min}.

To extend the q-region toward higher, we need to discriminate incoherent scattering from hydrogen in soft matters. SANS intensity $I(q)$ contains both of coherent $I_{coh}(q)$ and spin incoherent scattering $I_{inc}(q)$, which is given by independently summing, $I(q) = I_{coh}(q) + I_{inc}(q)$ (A-9)

It should be denoted that an incoherent scattering process flips the spin state of neutron π [61,62]. A method of polarization analysis discriminates spin flip and non-flip scattering processes ($I_{SF}(q)$ and $I_{NSF}(q)$). As shown in Fig. 14, a spin polarizer and analyzer (Heusler single crystal), allocated before and after the sample position, reflect neutrons of a peculiar spin state (up spin for example). By flipping the spin state of incident neutron, using a π flipper which is allocated at upper stream of sample position. $I_{SF}(q)$ and $I_{NSF}(q)$ are related to coherent and incoherent scattering as

$$I_{NSF}(q) = I_{coh}(q) + (1/3)\, I_{inc}(q) \tag{A-10}$$

and

$$I_{SF}(q) = (2/3)\, I_{inc}(q) \tag{A-11}$$

By experimentally observing $I_{SF}(q)$ and $I_{NSF}(q)$, we quantitatively separate $I_{coh}(q)$ and $I_{inc}(q)$. SANS-J-II spectrometer has a wide-angle detector with analyzer mirrors [63], which profits to perform the polarization analysis on the aqueous film system [64].

References

[1] C.H. Haigler, P.J. Weimer (Eds.), Biosynthesis and Biodegradation of Cellulose, Marcel Dekker Inc., New York, 1991.
[2] S. Koizumi, Y. Zhao, Y. Tomita, T. Kondo, H. Iwase, D. Yamaguchi, T. Hashimoto, Eur. Phys. J. E 26 (2008) 137–142.
[3] S. Koizumi, Y. Tomita, T. Kondo, T. Hashimoto, Macromol. Symp. 279 (1) (2010) 110–118.
[4] T. Hashimoto, S. Koizumi, Polym. Sci. 2 (2012) 381–398.
[5] Y. Zhao, S. Koizumi, D. Yamaguchi, T. Kondo, Eur. Phys. J. E 37 (2014).
[6] Y. Zhao, S. Koizumi, Eur. Polym. J. 66 (2015) 437–443.
[7] R. Malcolm Brown Jr., Inder M. Saxena, Plant Physiol. Biochem. 38 (2000) 57–67.
[8] Inder M. Saxena, R. Malcolm Brown Jr., Ann. Bot. 96 (2005) 9–21.
[9] H.G. Schild, Prog. Polym. Sci. 17 (1992) 163 and references therein.
[10] S. Hestrin, M. Schramm, Biochem. J. 58 (1954) 345.
[11] S. Koizumi, H. Iwase, J. Suzuki, T. Oku, R. Motokawa, H. Sasao, H. Tanaka, D. Yamaguchi, H.M. Shimizu, T. Hashimoto, Phys. B Condens. Matter 385–386 (2006) 1000–1006.
[12] S. Koizumi, H. Iwase, J. Suzuki, T. Oku, R. Motokawa, H. Sasao, H. Tanaka, D. Yamaguchi, H.M. Shimizu, T. Hashimoto, J. Appl. Crystallogr. 40 (2007) s474–s479.
[13] T. Imae, T. Kanaya, M. Furusaka, N. Torikai, Neutrons in Soft Matter, Wiley, 2011.
[14] D. Yamaguchi, S. Koizumi, R. Motokawa, T. Kumada, K. Aizawa, T. Hashimoto, Phys. B Condens. Matter 385–386 (2006) 1190–1193.
[15] S. Koizumi, T. Inami, Macromolecules 32 (1999) 5613–5621.
[16] P. Scherrer, Nachr. Ges. Wiss. Göttingen (1918) 98–100 26 September.
[17] J.S. Higgins, H.C. Benoît, Polymer and Neutron Scattering, Oxford, 1994.
[18] J.D. Watson, "Molecular Biology of the Gene", 3rd. ed. P69, Benjamin, 1976.
[19] Roe "Mehtods of X-Ray and Neutron Scattering in Polymer Science", New York Oxford, (2000).
[20] P.G. de Gennes, F. Brochard-Wyart, D. Quere, "Capillarity and Wetting Phenomena Drops, Bubbles, Perals, Waves" by, Springer Science, 2004.
[21] S. Hirotsu, J. Phys. Soc. Jpn. 56 (1987) 233–242.
[22] R.G. de Azevedo, L.P.N. Rebelo, et al., Fluid Phase Equilib. 185 (2001) 189–198.
[23] Y. Okada, F. Tanaka, Macromolecules 38 (2005) 4465–4471.
[24] B.M. Mulder, A.M.C. Emons, J. Math. Biol. 42 (2001) 261–289.
[25] T. Masui, S. Koizumi, T. Hashimoto, K. Shikinaka, A. Kakugo, J.P. Gong, Soft Matter

6 (2010) 2021–2030.
[26] Mohraz Ali, David B. Moler, Robert M. Ziff, Michael J. Solomon, Phys. Rev. Lett. 92 (15) (2004) 155503-1.
[27] H. Tanaka, S. Koizumi, T. Hashimoto, K. Kurosaki, S. Kobayashi, Macromolecules 40 (2007) 6304–6315.
[28] T. Hashimoto, H. Tanaka, S. Koizumi, K. Kurosaki, M. Ohmae, S. Kobayashi, Macromolecules 40 (2007) 406–409.
[29] T. Hashimoto, H. Tanaka, S. Koizumi, K. Kurosaki, M. Ohmae, S. Kobayashi, Biomacromolecules 7 (2006) 2479–2482.
[30] K. Yamauchi, H. Hasegawa, T. Hashimoto, H. Tanaka, R. Motokawa, S. Koizumi, Macromolecules 39 (2006) 4531–4539.
[31] N. Miyamoto, H. Inoue, S. Koizumi, T. Hashimoto, J. Appl. Crystallogr. 40 (2007) s568–s572.
[32] Y. Zhao, H. Tanaka, N. Miyamoto, S. Koizumi, T. Hashimoto, Macromolecules 42 (2009) 1739–1748.
[33] Y. Zhao, N. Miyamoto, S. Koizumi, T. Hashimoto, Macromolecules 43 (2010) 2948–2959.
[34] T. Terashima, R. Motokawa, S. Koizumi, M. Sawamoto, M. Kamigaito, T. Ando, T. Hashimoto, Macromolecules 43 (2010) 8218–8232.
[35] H. Iwase, S. Sawada, T. Yamaki, Y. Maekawa, S. Koizumi, J. Polym. Sci. J. Polym. Sci. (2011) 301807.
[36] R. Motokawa, Y. Iida, Y. Zhao, T. Hashimoto, S. Koizumi, Polym. J. 39 (2007) 1312–1318.
[37] R. Motokawa, S. Koizumi, T. Hashimoto, M. Annaka, T. Nakahira, Macromolecules 43 (2010) 752–764.
[38] H. Tanaka, S. Koizumi, T. Hashimoto, H. Itoh, M. Satoh, K. Naka, Y. Chujo, Macromolecules 40 (2007) 4327–4337.
[39] H. Tanaka, T. Hashimoto, S. Koizumi, H. Itoh, K. Naka, Y. Chujo, Macromolecules 41 (2008) 1815–1824.
[40] Y. Zhao, K. Saijo, M. Takenaka, S. Koizumi, T. Hashimoto, Macromolecules 42 (2009) 5272–5277.
[41] Y. Zhao, K. Saijo, M. Takenaka, S. Koizumi, T. Hashimoto, Polymer 50 (2009) 2696–2705.
[42] T. Kawakatsu, H. Tanaka, S. Koizumi, T. Hashimoto, J. Phys. Condens. Matter 18 (2006) s2499–s2512.
[43] Y. Iida, T. Kawakatsu, R. Motokawa, S. Koizumi, T. Hashimoto, Macromolecules 41 (2008) 9722–9726.
[44] J. Byrne, Neutron, Nuclei and Matter, an Explanation of the Physics and Slow Neutrons, IOP Publishing Ltd., 1994.
[45] S. Koizumi et al. submitted to J. Appl. Cryst.
[46] W. Schmatz, T. Springer, J. Shelton, K. Ibel, J. Appl. Crystallogr. 7 (1974) 96.
[47] In, France: K. Ibel, J. Appl. Crystallogr. 9 (1976) 296–309 In the United States: C. J. Glinka, J. M. Rowe and J. G. LARock, J. Appl. Crystallogr. 19, (1986) 427-439.
[48] V.F. Sears, Neutron Optics, Oxford University Press, New York, 1989.
[49] J.M. Carpenter, C.-K. Loong, Elements of Slow-Neutron Scattering". Cambridge, (2015).
[50] M.R. Eskildsen, P.L. Gammel, E.D. Issacs, C. Detlefs, K. Mortensen, D.J. Bishop, Nature 391 (5) (1998) 563–566.
[51] S.-M. Choi, J.G. Barker, C.J. Glinka, Y.T. Cheng, P.L. Gammel, J. Appl. Crystallogr. 33 (2000) 793–796.
[52] H. Frielinghaus, V. Pipich, A. Radulescu, M. Heiderich, R. Hanslik, K. Dahlhoff, H. Iwase, S. Koizumi, D. Schwahn, J. Appl. Crystallogr. 42 (2009) 681–690.
[53] The magnetic lens was a Stern–Gerlach experimental apparatus, R. Gahler, J. Kalus, W. Mampe, J. Phys. E Sci. Instrum. 13 (1980) 546 and is composed of a sextupole magnet and finished as a lens (T. Oku, H. Iwase, T. Sshinohara, S. Yamada, K. Hirota, S. Koizumi, J. Suzuki, T. Hashimoto and H.M. Shimizu, J. Appl. Crystallogr, 40, (2007b) s408-s413.
[54] P. Mikula, P. Lukos, F. Eichorn, J. Appl. Crystallogr. 21 (1988) 33.
[55] A. Brûlet, V. Thevenot, D. Lairez, S. Lecommandoux, W. Agut GUT, S.P. Armes, J. Du, S.J. Desert, Appl. Crystallogr. 41 (2008) 161.
[56] B. Alefeld, C. Hates, F. Mezai, D. Richter, T. Springer, Physica B 234–236 (1997) 1052.
[57] W.G. Bouman, J. Plomp, V.O. de Haan, W.H. Kraan, A.A.v. Well, K. Habicht, T. Keller, M.T. Rekveldt, Nucl. Instrum. Methods Phys. Res. 586 (2008) 9 and references cited therein.
[58] U. Bonse, M. Hart, Appl. Phys. Lett. 7 (1965) 238.
[59] D. Schwahn, A. Miksovsky, H. Rauch, E. Seidl, G. Zugarek, Nucl. Instrum. Methods Phys. Res. A239 (1985) 229–234.
[60] As a Japanese Textbook, Seiji Kikuta "X-Ray Diffraction and Scattering vol. 1, University of Tokyo Press, 1992 Experimental Techniques in Applied Physics.
[61] G.L. Squires, Introduction to the Theory of Thermal Neutron Scattering, 3rd., Cambridge University Press, 2012.
[62] W. Gavin, Williams "Polarized Neutron" Oxford Series on Neutron Scattering on Condensed Matter No.1 Oxford, (1988).
[63] H. Iwase, S. Koizumi, J. Suzuki, T. Oku, H. Sasao, H. Tanaka, H.M. Shimizu, T. Hashimoto, J. Appl. Crystallogr. 40 (2007) s414–s417.
[64] Y. Noda, D. Yamaguchi, A. Putra, S. Koizumi, Y. Sakaguchi, T. Oku, J. Suzuki, Phys. Proc. 42 (2013) 46–51.

Hierarchical structure of microbial cellulose and marvelous water uptake, investigated by combining neutron scattering instruments at research reactor JRR-3, Tokai

ORIGINALITY REPORT

17%	12%	16%	2%
SIMILARITY INDEX	INTERNET SOURCES	PUBLICATIONS	STUDENT PAPERS

MATCH ALL SOURCES (ONLY SELECTED SOURCE PRINTED)

2%

★ juser.fz-juelich.de

Internet Source

Exclude quotes	Off	Exclude matches	Off
Exclude bibliography	Off		